Springer

KSME

Journal of Mechanical Science and Technology 29 (10) (2015) 4143~4152
www.springerlink.com/content/1738-494x(Print)/1976-3824(Online)
DOI 10.1007/s12206-015-0908-1

Lifetime prediction for turbine discs based on a modified Walker strain model †

Zhiqiang Lv, Hong-Zhong Huang*, Huiying Gao, Fang-Jun Zuo and Hai-Kun Wang

Institute of Reliability Engineering, University of Electronic Science and Technology of China, Chengdu, Sichuan, 611731, China

(Manuscript Received September 23, 2014; Revised May 16, 2015; Accepted May 27, 2015)

Abstract

We created three-dimensional models of turbine disc and blades of a type of aero-engine according to their geometries. Extant studies show that low cycle fatigue is the main failure mechanism of turbine disc. By using a non-linear elastic-plastic finite element method, the static stress and strain state of the critically high stress regions, which can lead to operational failures, are determined. On the basis of stress-strain relation, a modified Walker strain life prediction model is proposed with no required knowledge on the mean stress correction. Then the predicted life data from the modified Walker strain model are compared with the testing results. After the verification, the modified Walker strain life prediction model and Miner's rule were applied to predict the lifetime of the turbine disc under various operating conditions.

Keywords: Turbine disc; Finite element method; Low cycle fatigue; Life prediction; Modified Walker strain model

1. Introduction

The main function of the turbine disc is to install blades and transmit power. During the operation of the aero-engine, the turbine disc endures substantial mechanical and thermal stresses due to the high rotational velocity and large temperature gradients. Generally, turbine disc failure mechanisms can be ascribed to Low cycle fatigue (LCF), fracture, yielding, creep, corrosion, erosion and wear [1]. Turbine disc is one of the critical components in an aero-engine [2]. Failures of turbine disc will affect the function of the aero-engine, and then it will further create a safety risk. In most cases, such failures will cause catastrophic consequences. Therefore, it is of turbine disc great importance to carry out a detailed reliability analysis on the strength and lifetime of turbine disc.

Much effort has been focused on the stress and failure analysis of the aero-engine turbine disc in literature. Meguid et al. [3] established a three-dimensional model of a turbine disc and took the effect of the interfacial friction between the turbine disc and attached blades into consideration. Cláudio et al. [4] applied finite element method to replace the time-consuming and expensive tests in real turbine discs. They used a crack propagation program to predict the fatigue life of turbine disc. Taking into the account the severe operating conditions of an aero-engine, Wu et al. [5] integrated the mechanical and thermal stresses into the life prediction model, and concluded that the life prediction of turbine's critical components is equivalent to predicting the crack nucleation and growth. Witek [1] utilized the finite element method to calculate the stress state and the stress intensity factor of the turbine disc, and plotted the fatigue crack growth curve of the turbine disc based on Paris-Erdogan equation.

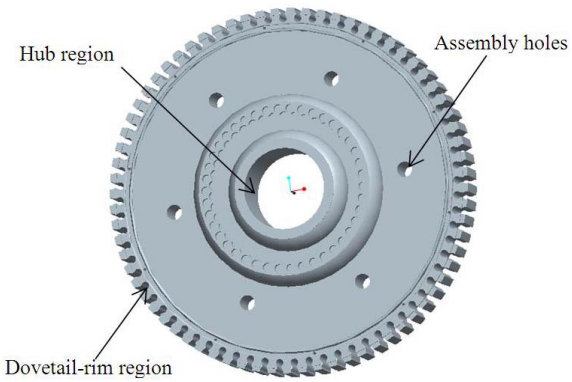

Fig. 1. The critical high stress regions of turbine disc.

There are three critical high stress regions in an aero-engine turbine disc (Fig. 1): the fir-tree rim region (dovetail-rim region), the assembly holes and the hub region [3, 6].

These three critical regions contain stress and strain concentrations due to the holes [7, 8]. The high stresses in these three critical regions are mainly caused by the large centrifugal force and the extreme thermal stresses of the aero-engine turbine disc itself.

*Corresponding author. Tel.: +86 28 6183 0248, Fax.: +86 28 6183 0227
E-mail address: hzhuang@uestc.edu.cn
† Recommended by Editor Chongdu Cho

Table 1. Mechanical properties of the disc material GH4133.

Temperature (°C)	Young modulus E (GPa)	Poisson's ratio	Coefficient of thermal expansion (10^{-6}/°C)	Density (kg/m^3)
20	223	0.36	12.0	8210
100	219	0.37	12.0	
200	214	0.34	12.9	
300	207	0.35	13.5	
400	203	0.35	13.9	
500	197	0.37	14.6	
600	190	0.35	15.0	
700	183	0.35	15.8	
800	176	0.39	16.6	

Table 2. Tensile properties of tangential specimen of the turbine disc.

Temperature (°C)	Ultimate strength σ_b (MPa)	Yield strength $\sigma_{0.2}$ (MPa)	Percentage elongation δ (/%)	Reduction of area ψ (/%)
20	1221	878	28	31
400	1079	694	24	31
500	1055	716	27	29
600	1030	692	24	29
650	1010	672	27	30
700	962	667	17	26
750	878	623	16	21
800	638	530	16	17

2. Finite element modeling

We created a three-dimensional model of a second stage low pressure turbine disc for a certain type of aero-engine. Both the static stress and the strain state of the critical high stress regions of the turbine disc were determined by the ANSYS program.

2.1 Material

The object of this study is a second stage low pressure turbine disc that is made of GH4133, one typical superalloy. The material properties of the GH4133 are listed in Tables 1 and 2 [9].

2.2 Structural features of turbine disc

The actual turbine disc analyzed in this paper has the following characteristics.

(1) There are 49 fir-tree mortises on the second stage low pressure turbine disc. For each fir-tree mortise, it can be installed with two blades.

(2) To have a more suitable blade consistency, the fir-tree mortises of the second stage low pressure turbine disc are chutes, as shown in Fig. 2.

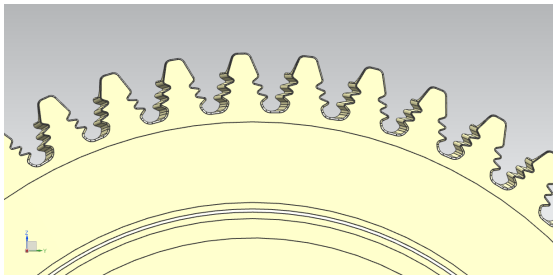

Fig. 2. The fir-tree mortises of the turbine disc.

2.3 Simplification of the three-dimensional model

The turbine disc has a complex structure with irregular shapes. When analyzing the local stress distribution using finite element method, some local features, such as fillet and chamfer, they have little influence on the stress and strain distribution of the whole turbine disc. However, these features will increase the difficulty in creating meshes. In the worst case, they lead to singular finite elements and wrong results. Therefore, before performing the finite element analysis of the turbine disc, the local features like fillet and chamfer are simplified in the three-dimensional model.

2.4 Three-dimensional model and elements

The second stage low pressure turbine disc in this paper is designed to be cyclically symmetric. Such a disc has a rotationally periodic structure. The whole turbine disc can be obtained through the simple rotations of one cyclic part of the turbine disc. Besides, the loads and constraints of the turbine disc are also symmetric. Hence, cyclic symmetry is applied here to the three-dimensional model of the turbine disc.

As mentioned in Sec. 1, an aero-engine turbine disc has three critical high stress regions: the fir-tree rim region, the assembly holes and the hub region. For the second stage low pressure turbine disc, there are 49 fir-tree mortises and 6 assembly holes. Thus there is no appropriate common divisor of the number of the fir-tree mortises and the assembly holes. Also considering that the cyclical symmetry of the turbine disc reduces the computation burden, the fir-tree rim region and the assembly holes were analyzed separately in this paper. The detailed information is given below:

(1) When analyzing the assembly holes, a simplified three-dimensional model of the 1/6 turbine disc segment was created, and the fir-tree mortises structure were removed from the rim of the turbine disc (see Fig. 3).

(2) When analyzing the fir-tree rim region, a simplified version of the three-dimensional model of the 1/49 turbine disc segment was created. The assembly hole was simplified, and the contact analysis [10] between the turbine disc and the blades was done as shown in Fig. 4.

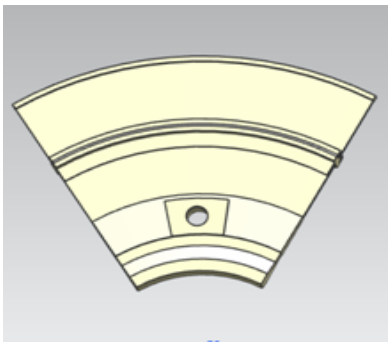

Fig. 3. The 1/6 turbine disc segment without fir-tree mortises structure.

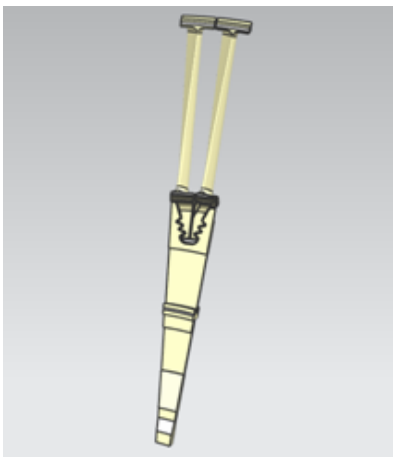

Fig. 4. The 1/49 turbine disc segment without assembly holes.

To ensure the mesh quality of the three-dimensional model and avoid excessive calculations, the finite element mesh model of the turbine disc is create by using a density transition approach. In the stress concentration regions, such as the fir-tree rim region, the assembly holes and the hub region, 10-node tetrahedral units were used to divide the dense grids. In the turbine disc that has regular structure and low stress gradient, 8-node hexahedral units were used to divide the sparse grids.

2.5 Loading

During the operation of an aero-engine, the turbine disc is subjected to a mixed load: centrifugal forces, thermal stresses, aerodynamic forces and vibratory stresses. Of course, high speed results in large centrifugal forces and high thermal gradients result in thermal stresses. Among them, the aerodynamic forces and vibratory stresses have little effect on the static strength of the turbine disc. Therefore, when analyzing the turbine disc with finite element method, the centrifugal forces and thermal stresses are the main consideration.

The speed spectrum of the turbine disc is determined by the flight mission, and it consists of three parts [11]: low frequency cycle, full throttle cycle and cruise cycle. Any speed spectrum can be considered as a combination of these three basic cycles. The speed spectrum of the turbine disc is shown in Table 3.

Table 3. Speed spectrum of the turbine disc under 800 h.

Working cycles	Number of cycles	Rotational speed (rpm)
Low frequency cycle	1220	0-10870-0
Full throttle cycle	1850	3360-10870-3360
Cruise cycle	17320	9600-10870-9600

Table 4. Temperature data points of the turbine disc.

X (m)	Y (m)	Z (m)	Temperature (K)
1.03680e-001	1.03430e-002	1.08493e-001	4.21930e+002
1.03700e-001	1.03430e-002	1.08493e-001	4.23193e+002
1.06580e-001	1.02513e-002	1.06502e-001	4.03822e+002
1.06489e-001	1.02233e-002	1.06211e-001	4.03912e+002
1.06080e-001	1.01555e-002	1.05507e-001	4.08031e+002
1.06189e-001	1.02233e-002	1.06211e-001	4.06288e+002
1.06280e-001	1.04430e-002	1.08493e-001	4.06127e+002
1.10470e-001	1.02233e-002	1.06211e-001	4.20925e+002
1.10080e-001	1.02513e-002	1.06502e-001	4.20244e+002
1.10170e-001	1.02233e-002	1.06211e-001	4.20269e+002

The temperature spectrum is derived based on the measurement data. In this study, the temperature spectrum of the turbine disc was loaded on the three-dimensional model by ANSYS parametric design language. For each basic cycle mentioned above, there are 100000 temperature data points of the turbine disc. Table 4 shows part of the temperature data points under full throttle cycle, where X, Y and Z represent the coordinate value of a point of the three-dimensional model.

2.6 Stress and strain analysis of the turbine disc

As it mentioned in Sec. 2.4, the fir-tree rim region and the assembly holes were analyzed separately by using finite element method.

For the three-three-dimensional model in Fig 3, the 1/6 turbine disc segment is subjected to a combination of centrifugal forces and thermal stresses. The centrifugal forces include three parts: centrifugal forces produced by the 1/6 turbine disc segment itself, centrifugal forces produced by the removed fir-tree mortises structure, and centrifugal forces produced by the blades. In the program ANSYS, the former was loaded into the three-dimensional model in the form of rotational speed, and the latter two were loaded into the three-dimensional model in the form of pressure. The thermal stresses were loaded into the three-dimensional model by inputting the temperature data with ANSYS parametric design language. Then the finite element analysis results of the 1/6 turbine disc segment under different working cycles are shown in Figs. 5-7 below.

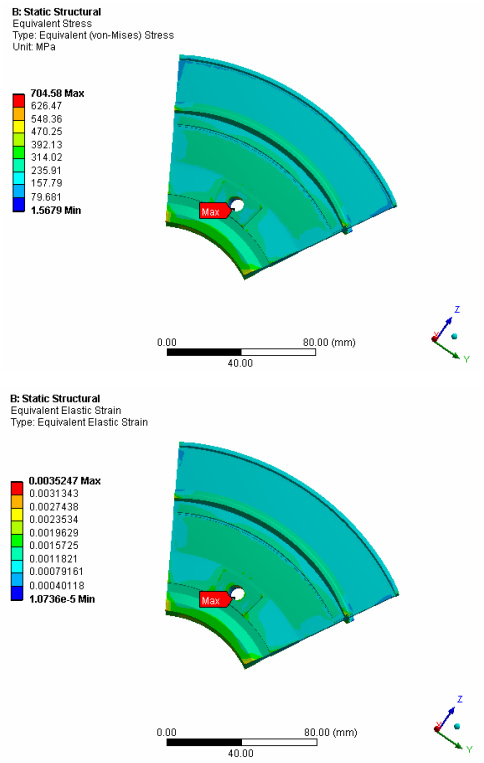

Fig. 5. Static stress and strain state under low frequency cycle.

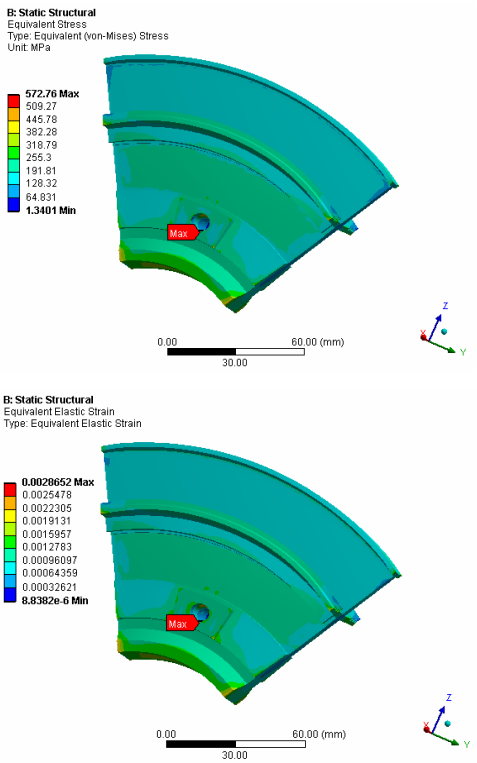

Fig. 7. Static stress and strain state under cruise cycle.

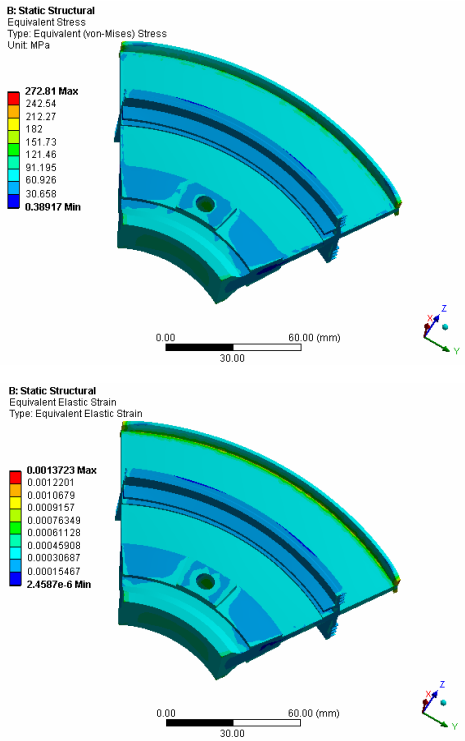

Fig. 6. Static stress and strain state under full throttle cycle.

As Figs. 5-7 show, for the 1/6 turbine disc segment, the maximum stress and strain concentration occurs on the assembly hole. The stress and strain concentration locations can determine the lifetime of 1/6 turbine disc segment so the most critical high stress region of the 1/6 turbine disc segment is located in the assembly hole.

Similarly, for the three-dimensional model in Fig. 4, the simplified 1/49 turbine disc segment is also subjected to a combined load of centrifugal forces and thermal stresses. The centrifugal forces were loaded on the three-dimensional model in the form of rotational speed. And the thermal stresses were loaded into the three-dimensional model by inputting the temperature data with ANSYS parametric design language. Besides, the contact between turbine disc and blade was considered and a friction coefficient of 0.15 was defined. The finite element analysis results of the 1/49 turbine disc segment under different working cycles are shown in Figs. 8-10, respectively.

According to Figs. 8-10, for the 1/49 turbine disc segment, after the assembly hole was simplified from the structure, the maximum stress and strain concentration is located in the corner of the 3rd lower slot of the fir-tree rim region of the turbine disc. As mentioned above, the stress and strain concentration locations can determine the lifetime of structures, which means that the most critical high stress region of the 1/49 turbine disc segment is the fir-tree rim region.

The static stress and strain distribution of the 1/6 turbine disc segment and the 1/49 turbine disc segment are shown in Figs. 5-10. Here, according to these figures, the maximum stress and strain values of the most critical high stress regions of 1/6 turbine disc segment and the 1/49 turbine disc

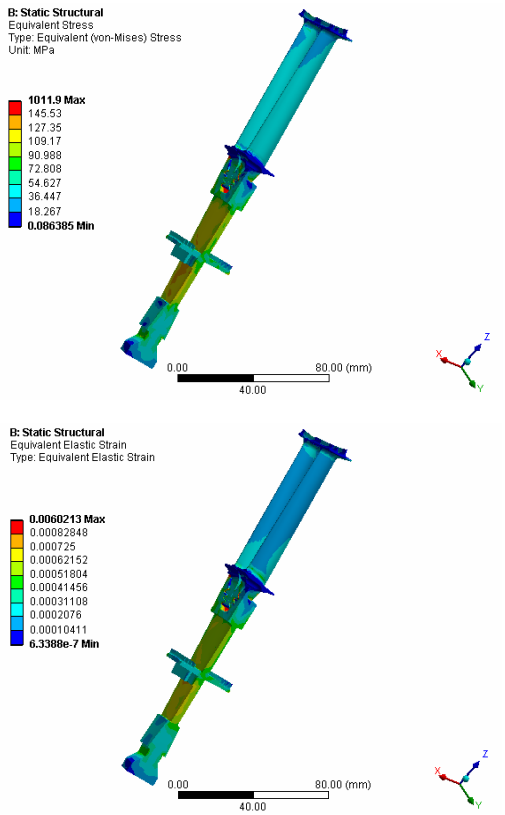

Fig. 8. Static stress and strain state under low frequency cycle.

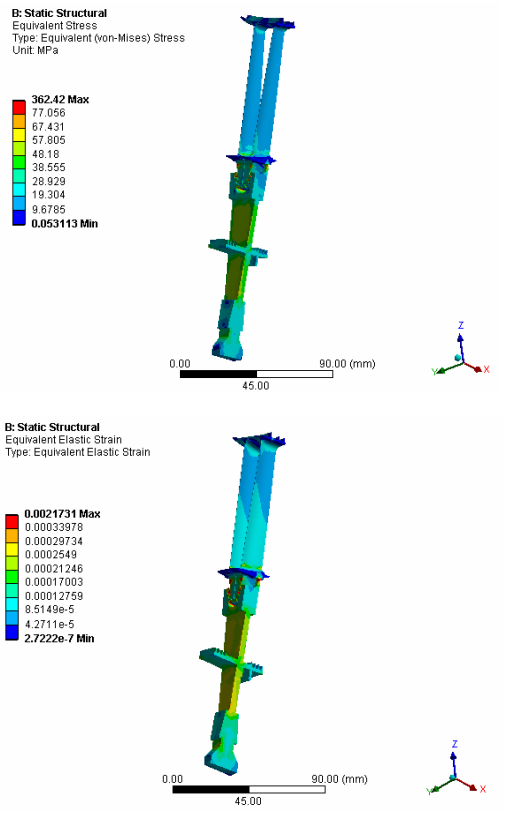

Fig. 9. Static stress and strain state under full throttle cycle.

Table 5. Stress and strain distribution of the 1/6 turbine disc segment.

Working cycles	Maximum stress σ_{max} (MPa)	Minimum stress σ_{min} (MPa)	Total strain range $2\varepsilon_a$
Low frequency cycle	704.58	0	3.5247e-003
Full throttle cycle	704.58	272.81	2.1524e-003
Cruise cycle	704.58	572.76	6.595e-004

Table 6. Stress and strain distribution of the 1/49 turbine disc segment.

Working cycles	Maximum stress σ_{max} (MPa)	Minimum stress σ_{min} (MPa)	Total strain range $2\varepsilon_a$
Low frequency cycle	1011.90	0	6.0213e-003
Full throttle cycle	1011.90	362.42	3.8482e-003
Cruise cycle	1011.90	787.55	1.3348e-003

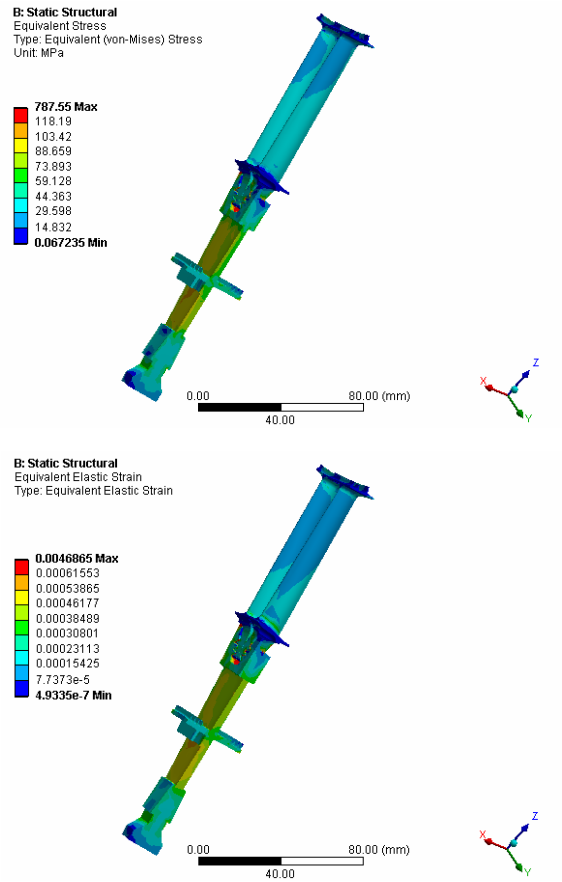

Fig. 10. Static stress and strain state under cruise cycle.

segment under the three basic working cycles are listed in Tables 5 and 6, respectively.

As concluded above, for the 1/6 turbine disc segment, its most critical high stress region is the assembly hole, and for the 1/49 turbine disc segment, its most critical high stress region is the fir-tree rim region. However, under the same

operating conditions, the maximum stress and strain values of the most critical high stress regions of 1/6 turbine disc segment and the 1/49 turbine disc segment are different. According to the finite element analysis results in Tables 5 and 6, under the same basic working cycle, the maximum stress and strain values of the fir-tree rim region are larger than the assembly hole. It means that the fir-tree rim region has less lifetime than the assembly hole. Besides, both the fir-tree rim region and the assembly hole are more critical regions than the hub region according to Figs. 5-10. Therefore, here we can conclude that, among the three critical high stress regions of the second stage low pressure turbine disc, the most critical high stress region is the fir-tree rim region, the second critical high stress region is the assembly holes, and the third critical high stress region is the hub region. Then in the next section, the life prediction analysis of the turbine disc is mainly based on the stress and strain values of the fir-tree rim region.

3. Life prediction analysis of the turbine disc

For the turbine disc, it is subjected to very high centrifugal forces and thermal stresses. Under the operating conditions, the magnitude of the high stress is beyond the elastic range of the material GH4133. Hence, LCF is the main failure mechanism that limits the service life of the turbine disc [12-14]. Due to the importance of the life prediction of the turbine disc, much work has been done to seek accurate LCF life prediction models for the turbine disc [5, 15-18]. For the turbine disc, there are some characteristics associated with the LCF failure [19]. The LCF failure characteristics are summarized below.

(1) The fatigue loading of the turbine disc is asymmetrical. During the operation of the turbine disc, the load parameters, such as rotation speed and temperature are asymmetrical.

(2) According to statistics, the time to failure of the turbine disc lies within the range of 10^3-10^5.

However, for the material of the turbine disc, the fatigue performance data are predominately obtained under symmetrical cyclic loading. Therefore, when predicting the turbine disc life, the fatigue performance data need to be modified with mean stress correction procedures, but different modified methods often lead to different prediction results [20, 21].

To avoid a large discrepancy of the life prediction results caused by different modified methods and also based on the characteristics of the LCF failure of the turbine disc, a modified Walker strain life prediction model was proposed to predict the life of the turbine disc in the following section.

3.1 The modified Walker strain life prediction model

The Walker strain life prediction model defines an equivalent local strain ε_{eq} [15, 22], which had taken the effect of mean stress correction into consideration. The mathematical expression of ε_{eq} is

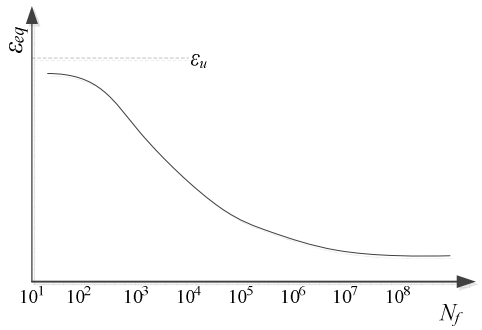

Fig. 11. Schematic illustration of regressed inverse hyperbolic tangent curve.

$$\varepsilon_{eq} = (2\varepsilon_a)^m \left(\sigma_{\max}/E\right)^{1-m}, \tag{1}$$

where ε_{eq} is equivalent local strain, ε_a is local strain amplitude, m is material constant, and for the GH4133, m = 0.55 [19], $\sigma_{\max}$ is maximum nominal stress, and E is Young modulus.

To implement the usage of Walker strain life prediction model, Jaske et al. [22] established a functional form by fitting experiment data. The functional form is given as

$$\log N_f = A_0 + A_1 \tanh^{-1}\left[\frac{\log\left(\varepsilon_u\varepsilon_e/\varepsilon_{eq}^2\right)}{\log\left(\varepsilon_u/\varepsilon_e\right)}\right], \tag{2}$$

where N_f is the number of cycles to failure, A_0 is the first regression coefficient, A_1 is the second regression coefficient, ε_u is the upper limit of inverse hyperbolic tangent function, and ε_e is the lower limit of inverse hyperbolic tangent function. As illustrated in Fig. 11, the values of ε_u and ε_e were determined as

$$\varepsilon_u = \varepsilon_{eq}|_{N_f=10} + 0.0025, \tag{3}$$

$$\varepsilon_e = \varepsilon_{eq}|_{N_f=10^8} - 0.0005. \tag{4}$$

According to Fig. 11, the Walker strain life prediction curve has a broad life range. And it has been verified that the Eq. (2) can be well used for life prediction of different materials [22]. Besides, for the equivalent local strain ε_{eq}, it had taken the effect of mean stress correction into consideration; therefore, there is no need of mean stress correction procedures for Eq. (2). However, in practical applications, it is difficult to obtain the values of A_0, A_1, ε_u and ε_e due to the lack of real testing data. All of these limit the wide use of the Walker strain life model. Therefore, in this section, the Walker strain life model was simplified and improved.

As shown in Eq. (2) and Fig. 11, for the N_f, in the range of 10^3-10^6, the trend of the regressed inverse hyperbolic tangent curve is relatively simple. Also, the failure range of the LCF

Table 7. Experimental data under T = 250°C and R = -1.

ε_a	σ_{max} (MPa)	N_f	ε_{eq}
0.00318	666	24766	0.0047
0.00422	821	7998	0.0060
0.00483	892	5291	0.0067
0.00542	936	4164	0.0073
0.00697	985	1782	0.0085
0.00825	1040	864	0.0096

Table 8. Experimental data under T = 400°C and R = 0.

ε_a	σ_{max} (MPa)	N_f	ε_{eq}
0.006	880	1703	0.0076
0.005	826	4023	0.0067
0.004	751	6915	0.0057
0.0035	718	12141	0.0051
0.003	681	20421	0.0046
0.0025	645	35620	0.0041

Table 9. Experimental data under T = 400°C and R = -1.

ε_a	σ_{max} (MPa)	N_f	ε_{eq}
0.007	916	1043	0.0084
0.005	838	3489	0.0067
0.004	741	8259	0.0056
0.0035	690	13678	0.0051
0.003	597	25100	0.0044
0.0025	502	28402	0.0036

Table 10. Experimental data under T = 500°C and R = -1.

ε_a	σ_{max} (MPa)	N_f	ε_{eq}
0.007	868	741	0.0083
0.005	782	3455	0.0066
0.004	714	7248	0.0052
0.0035	653	12426	0.0050
0.003	566	23459	0.0043
0.00251	483	55499	0.0036

of turbine disc is basically in 10^5-10^6. Hence, it is feasible to use a more concise functional form which has less parameter to fit the experimental data in the life range of 10^3-10^6. The experimental data [19] of the material GH4133 under different temperature T and stress ratio R are shown in Tables 7-10, where ε_a, σ_{max}, and N_f are test data, ε_{eq} is caculated by Eq. (1).

Then, by fitting the experimental data ε_{eq} and N_f in Tables 7-10, we can get the fitted curve in Fig. 12. It has the form of an exponential function, and its mathematical expression is given as

$$\varepsilon_{eq} = 0.004212e^{-0.0002079N_f} + 0.005178e^{-0.000007551N_f} . \quad (5)$$

Table 11. Experimental data and predicted results under T = 250°C and R = -1.

ε_a	σ_{max} (MPa)	ε_{eq}	N_t	N_f
0.00317	662	0.004783207	18997	15368
0.00421	826	0.006176560	7950	5938
0.00418	836	0.006185720	6250	5907
0.00424	841	0.006251150	9525	5688
0.00424	801	0.006115562	4992	6151
0.00485	903	0.006949730	5862	3784
0.00482	896	0.006901841	4669	3896
0.00484	894	0.006910625	5077	3875
0.00482	898	0.006908770	5431	3879
0.00481	872	0.006810244	5418	4114
0.00544	951	0.007577241	3337	2515
0.00540	917	0.007423920	3599	2798
0.00543	951	0.007569577	3953	2529
0.00538	930	0.007455866	4799	2738

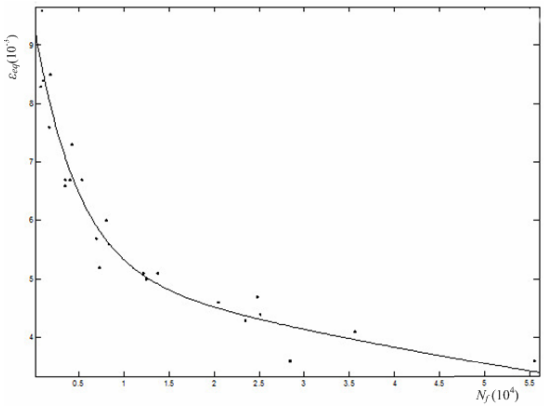

Fig. 12. The fitted curve of ε_{eq} and N_f.

3.2 Verification of the modified model

To assess the prediction accuracy of the modified model, in this section, an evaluating parameter of life assessment called scatter band is used. The scatter band of a specified factor s is defined as below [23].

$$\frac{1}{s} \le \frac{N_f}{N_t} \le s . \quad (6)$$

where N_f is the predicted value, and N_t is the experimental value.

Then two categories of experimental data [19] from material GH4133 under different temperature and stress ratio are used to verify the modified model, as shown in Tables 11 and 12 and Figs. 13 and 14.

For the modified model Eq. (5), it is not only a simplified form of Eq. (2) in the life range of 10^3-10^6, but also can be well fitted with the original model in the life range of 10^3-10^6.

Table 12. Experimental data and predicted results under T = 400°C and R = 0.

ε_a	σ_{max} (MPa)	ε_{eq}	N_t	N_f
0.006	863	0.008084	1534	1679
0.006	896	0.008222	1871	1472
0.005	802	0.007076	4244	3503
0.005	830	0.007186	4293	3270
0.004	780	0.00618	7533	5926
0.004	757	0.006098	6703	6214
0.0035	704	0.005484	11457	9013
0.0035	735	0.005591	10734	8417
0.003	714	0.00507	18465	12065
0.003	686	0.00498	19411	12959
0.0025	651	0.0044	26570	22698
0.0025	659	0.004424	29960	22117

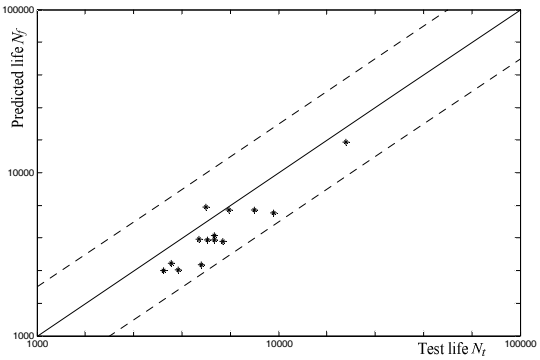

Fig. 13. Predicted life vs. tested life under T = 250°C and R = -1.

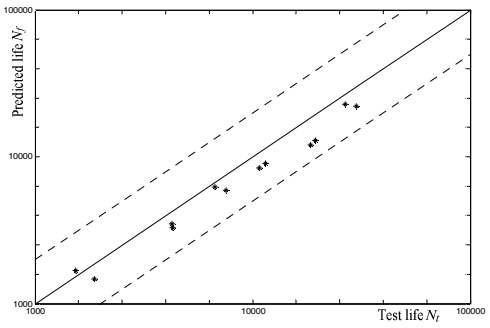

Fig. 14. Predicted life vs. tested life under T = 400°C and R = 0.

For the regressed inverse hyperbolic tangent curve in Fig. 11, due to the equivalent local strain ε_{eq}, it had taken the effect of mean stress correction into consideration. Therefore, for the modified model, although there are no mean stress correction procedures, in reality, the fitted curve in Fig. 12 is a curve which has been corrected of mean stress; this will guarantee the accuracy of the modified model. Then according to Tables 11 and 12 and Figs. 13 and 14, all the predicted results fall into a range within a scatter band of ±2, and nearly 80% of the predicted results fall into a range within a scatter band of ±1.5.

Table 13. Life prediction results of the modified model.

Parameters	Working cycles		
	Low frequency cycle	Full throttle cycle	Cruise cycle
Rotational speed (rpm)	0-10870-0	3360-10870-3360	9600-10870-9600
Number of cycles n_i	1220	1850	17320
E (GPa)	205	199	200
σ_{max} (MPa)	1011.90	1011.90	1011.90
σ_{min} (MPa)	0	362.42	787.55
ε_a	3.01e-003	1.92e-003	6.67e-004
ε_w	0.005506	0.00436	0.00243
N_{fi}	8885	23701	100189

And comparison between the test data and the predicted results by the modified model in Figs. 13 and 14 shows that the prediction results are in good agreement with the test data.

3.3 Life prediction of the turbine disc

As it mentioned in Sec. 2.6, the most critical high stress region of the turbine disc is the fir-tree rim region. Therefore, in this section, based on the stress analysis results (Table 6) of the 1/49 turbine disc segment and the modified Walker strain life prediction model (Eqs. (1) and (5)), we can estimate the turbine disc life under different working cycles, as shown in Table 13.

Then, we can get the turbine disc damage under different cycles by using Miner's rule [24], which can be expressed as

$$D = \sum_{i=1}^{n} \frac{n_i}{N_i} . \tag{7}$$

Based on Table 13, the total damage of turbine disc is

$$\begin{aligned} D &= \sum_{i=1}^{n} \frac{n_i}{N_i} \\ &= \frac{n_1}{N_{f1}} + \frac{n_2}{N_{f2}} + \frac{n_3}{N_{f3}} \\ &= \frac{1220}{8885} + \frac{1850}{23701} + \frac{17320}{100189} \\ &= 0.3883. \end{aligned} \tag{8}$$

Also, according to Table 3, the speed spectrum of the turbine disc is under the time of 800h; therefore, the life of the turbine disc is

$$\begin{aligned} T &= 800 \times \frac{1}{D} \\ &= 800 \times \frac{1}{0.3883} \\ &= 2060\text{h}. \end{aligned} \tag{9}$$

4. Conclusions

This paper leverages the finite element method to identify the critical high stress regions of the turbine disc, and further determine the static stress and strain state of turbine discs. The analysis shows that the most critical high stress region of the turbine disc is the fir-tree rim region, followed by the assembly holes and the hub region. To minimize the dispersion of the life prediction caused by the effects of mean stress correction, we have proposed a modified Walker strain life prediction approach. On the basis of the finite element analysis results, the modified Walker strain life prediction model and Miner's rule, the life of the turbine disc was obtained. The modified model was compared with the actual lifetime data generated from turbine discs tests. It is concluded that the prediction is in good agreement with the actual test data. In the future, application of the proposed model to life prediction for different parts of aero-engine needs further study.

Acknowledgment

This research was partially supported by the National Natural Science Foundation of China under the contract number U1330130.

Nomenclature

E	: Young modulus
σ_b	: Ultimate strength
$\sigma_{0.2}$	: Yield strength
δ	: Percentage elongation
ψ	: Reduction of area
σ_{max}	: Maximum stress
σ_{min}	: Minimum stress
$2\varepsilon_a$	: Total strain range
ε_{eq}	: Equivalent local strain
ε_a	: Local strain amplitude
m	: Material constant
N_f	: Number of cycles to failure
A_0	: First regression coefficient
A_1	: Second regression coefficient
ε_u	: Upper limit of inverse hyperbolic tangent function
ε_e	: Lower limit of inverse hyperbolic tangent function
R	: Stress ratio

References

[1] L. Witek, Numerical simulation of fatigue fracture of the turbine disc, *Fatigue of Aircraft Structures*, 1 (4) (2012) 114-122.

[2] G. F. Harrison and W. J. Evans, A review of fatigue assessment procedures for aeroengine fracture critical components, *J. of the Engineering Integrity Society* (2000).

[3] S. A. Meguid, P. S. Kanth and A. Czekanski, Finite element analysis of fir-tree region in turbine discs, *Finite Elements in Analysis and Design*, 35 (4) (2000) 305-317.

[4] R. A. Cláudio, C. M. Branco and E. C. Gomes, Life prediction of a gas turbine disc using the finite element method, *Eighth Portuguese Conference on Fracture* (2002).

[5] X. Wu, W. Beres and S. Yandt, Challenges in life prediction of gas turbine critical components, *Canadian Aeronautics and Space J.*, 54 (2) (2008) 31-39.

[6] L. Witek, Failure analysis of turbine disc of an aero engine, *Engineering Failure Analysis*, 13 (1) (2006) 9-17.

[7] Z. Yang, C. B. Kim and C. Cho, The concentration of stress and strain in finite thickness elastic plate containing a circular hole, *International J. of Solids and Structures*, 45 (3) (2008) 713-731.

[8] S. J. Kim, S. Y. Han and E. S. Shin, Micromechanics-based evaluation of the poroelastic effect and stress concentration in thermochemically-decomposed composites, *JMST*, 27 (10) (2013) 3139-3147.

[9] The Editorial Committee of China Aeronautical Materials Handbook, *China Aeronautical Materials Handbook,* Beijing, China (2002).

[10] H. Ou, B. Lu and Z. S. Cui, A direct shape optimization approach for contact problems with boundary stress concentration, *JMST*, 27 (9) (2013) 2751-2759.

[11] C. H. Tao, P. D. Zhong and R. Z. Wang, *Failure analysis and prevention for rotor in aero-engine*, Beijing, China (2008).

[12] C. L. Liu, Reliability analysis for an aero engine turbine disk under low cycle fatigue condition, *Acta Metallurgica Sinica*, 17 (4) (2009) 514-520 (In English).

[13] G. Harrison, Modes of gas turbine component life consumption in recommended practices for monitoring gas turbine engine life consumption, *RTO Technical Report 28 (RTO-TR-28, AC/323/(AVT)TP/22)* (2000).

[14] L. P. Gan, H. Z. Huang and S. P. Zhu, Fatigue reliability analysis of turbine disk alloy using saddlepoint approximation, *International J. of Turbo & Jet-engines*, 30 (3) (2013) 217-229.

[15] K. Walker, The effects of stress ratio during crack propagation and fatigue for 2024-t3 and 7075-t6 aluminum, *Effect of Environment and Complex Load History on Fatigue Life*, ASTM STP 462, American Society of Testing and Materials (1970) 1-14.

[16] K. N. Smith, P. Watson and T. H. Topper, A stress-strain function for the fatigue of metals, *J. of Materials*, 5 (4) (1970) 767-768.

[17] M. E. Melis, E. V. Zaretsky and R. August, Probabilistic analysis of aircraft gas turbine disk life and reliability, *Journal of Propulsion and Power*, 15 (5) (1999) 658-666.

[18] S. P. Zhu, H. Z. Huang and L. P. He, A generalized energy-based fatigue–creep damage parameter for life prediction of turbine disk alloys, *Engineering Fracture Mechanics*, 90 (2012) 89-100.

[19] W. G. Wang, *Research on prediction model for disc lcf life and experiment assessment methodology*, Nanjing University of Aeronautics and Astronautics (2006).

[20] S. M. H Kabir and T. Yeo, Fatigue behavior of an austenitic steel of 300-series under non-zero mean loading, *JMST*, 26 (1) (2012) 63-71.
[21] S. P. Zhu, H. Z. Huang and Z. L. Wang, Fatigue life estimation considering damaging and strengthening of low amplitude loads under different load sequences using fuzzy sets approach, *International J. of Damage Mechanics*, 20 (6) (2011) 876-899.
[22] C. E. Jaske, C. E. Feddersen and K. B. Davis, Analysis of fatigue, *Fatigue Crack Propagation and Fracture Data*, NASA CR-132332 (1973) 49-54.
[23] J. H. Park and J. H. Song, Detailed evaluation of methods for estimation of fatigue properties, *International J. of Fatigue*, 17 (5) (1995) 365-373.
[24] M. A. Miner, Cumulative damage in fatigue, *J. of Applied Mechanics*, 12 (3) (1945) 159-164.

Zhiqiang Lv is currently a Ph.D. candidate in Mechanical Engineering at the University of Electronic Science and Technology of China. His research interests concern fatigue life prediction and fatigue reliability.

Hong-Zhong Huang is a Professor of the School of Mechanical, Electronic, and Industrial Engineering, at the University of Electronic Science and Technology of China. He received a Ph.D. in Reliability Engineering from Shanghai Jiaotong University, China and has published in the fields of reliability engineering, optimization design, fuzzy sets theory, and product development.

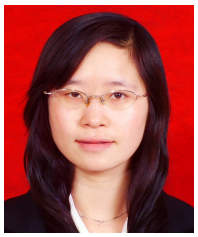

Huiying Gao is currently a Ph.D. candidate in Mechanical Engineering at the University of Electronic Science and Technology of China. Her research interests include fatigue strength evaluation, fatigue life prediction and fatigue reliability analysis.

Fang-Jun Zuo is a doctoral candidate in University of Electronic Science and Technology of China. Her research interests include fatigue life prediction and design for reliability.

Hai-Kun Wang is currently a Ph.D. candidate in Mechanical Engineering at the University of Electronic Science and Technology of China. He received his M.S. in Vehicle Engineering from the South China University of Technology. His research interests include reliability analysis, maintenance decisions, prognostics and health management.